Applied Catalysis B: Environmental 197 (2016) 184–197

Contents lists available at ScienceDirect

Applied Catalysis B: Environmental

journal homepage: www.elsevier.com/locate/apcatb

Elucidating the interaction between Ni and CeO_x in ethanol steam reforming catalysts: A perspective of recent studies over model and powder systems

Zongyuan Liu[a,b], Sanjaya D. Senanayake[a,*], José A. Rodriguez[a,b,*]

[a] Chemistry Department, Brookhaven National Laboratory, Upton, NY, 11973, United States
[b] Department of Chemistry, SUNY Stony Brook, Stony Brook, NY, 11794, United States

ARTICLE INFO

Article history:
Received 16 December 2015
Received in revised form 19 February 2016
Accepted 5 March 2016
Available online 8 March 2016

Keywords:
Ceria
Nickel
Ethanol steam reforming
Hydrogen generation
Water

ABSTRACT

Bulk metallic nickel is a poor catalyst for the reforming of oxygenates being deactivated by the deposition of coke. In contrast, Ni-ceria is an active system for the catalytic extraction of H_2 from the ethanol steam reforming reaction (ESR, $C_2H_5OH + 3H_2O \leftrightarrow 2CO_2 + 6H_2$). Numerous studies, with model (well-defined crystal surfaces) and technical (high surface area powders) catalysts, have been devoted to understand the fundamental role of each catalyst component, the performance of adjacent sites in the metal-oxide interface, and the complex mechanistic steps that convert two oxygenated reactants (ethanol and H_2O) into H_2. The size and low loading of Ni on ceria facilitate metal-oxide support interactions that probably enhance the reactivity of the system. To establish the precise role of both Ni and Ce is challenging. However it is clear that both Ni and Ce are associated with the dissociation of H_2O (OH + H), while ceria readily adsorbs and partially dissociates ethanol (i.e. ethoxy formation). The most difficult step of C—C bond dissociation likely occurs only on Ni or at the Ni-Ce interface. H_2O and OH remain as important agents for the prevention of excess C build up during the C—H/C—C dissociation process. Often, deactivation upon C build up, is a direct result of Ni sintering and decoupling of the Ni-Ce interactions. One strategy to maintain good activity and stability is to protect the Ni-Ce interaction, and this can be achieved through the use of solid solutions ($Ce_{1-x}Ni_xO_{2-y}$) or by employing stabilizing agents such as W ($Ni_xW_yCe_zO_2$). In this article, we present and discuss the most recent work for the ESR reaction and show the important role of ceria which participates directly in the reaction and also enhances catalytic activity through metal-support interactions.

1. Introduction

Ethanol steam reforming remains a classical prototype conversion reaction that is important for the efficient transformation of oxygenates into H_2, a process with great promise for fuel conversion for both large applications and small devices [1–3]. Numerous strategies have been adopted to screen for the best catalysts for this reaction, with careful consideration of element selection [4–13], sizes of metals [14–17], oxide support composition/architecture [18–28] and reaction conditions [29–32]. However, numerous challenges remain as obstacles to effective deployment in technical applications, some of which can only be mitigated through an improved understanding of the fundamental nature of the active catalyst and the reaction mechanism [1,3].

In the past several years, Ni has been used as a very promising candidate for this reaction comparable to noble metals such as Rh, Pt or Pd in terms of activity and selectivity [4,33,34]. Key properties of Ni allow for it to be used in the ESR process, including its ability to activate the C—C and C—H bonds in ethanol. However, drawbacks in the performance of Ni-based catalysts are their high propensity to yield methane as a reaction product and favoring C build up (i.e. coke formation), leading to a loss in selectivity and activity [1]. Three approaches can be followed to improve the performance of Ni in the ESR process. First, by preparing Ni as small nanoparticles, strong bulk effects can be mitigated [35]. Second, further enhancement can be achieved by coupling Ni with reducible oxide supports, such as ceria, which can influence catalytic chemistry through strong metal-support interactions [33,35–37]. And third, alloying Ni with other metals such as Pd, Pt or Rh, or the addi-

* Corresponding author.
E-mail addresses: ssenanay@bnl.gov (S.D. Senanayake), rodrigez@bnl.gov (J.A. Rodriguez).

http://dx.doi.org/10.1016/j.apcatb.2016.03.013
0926-3373/

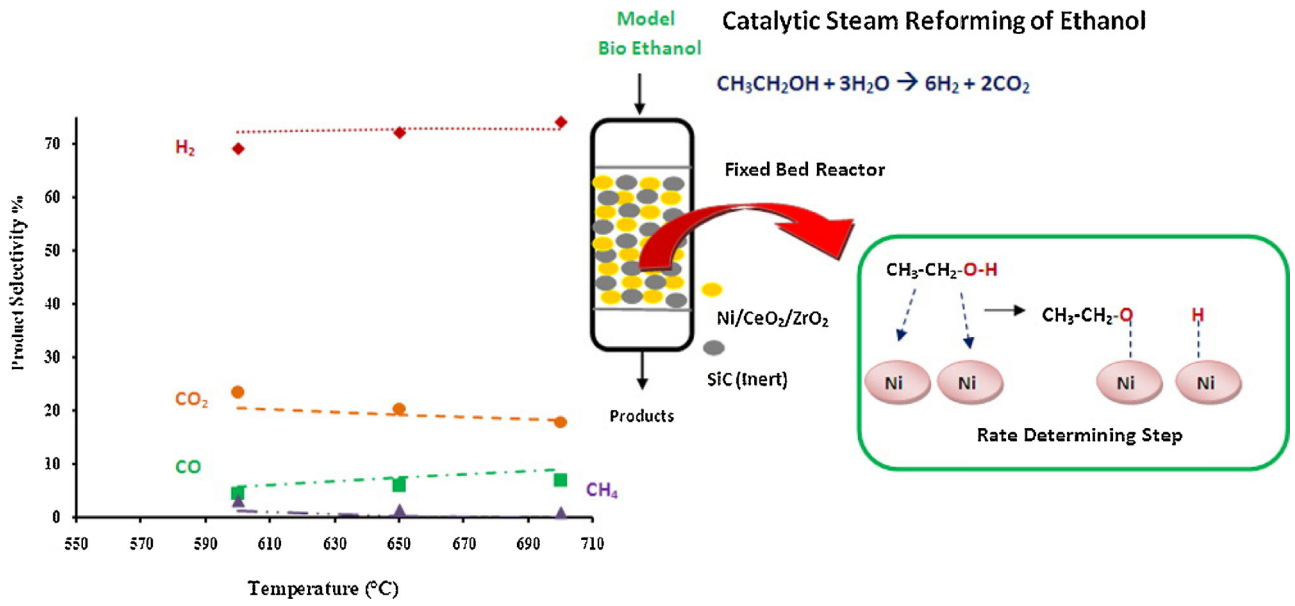

Fig. 1. Production of hydrogen after performing the ESR reaction on a Ni-ceria-zirconia catalyst. Taken from Ref. [45]. Copyright 2013 by the American Chemical Society.

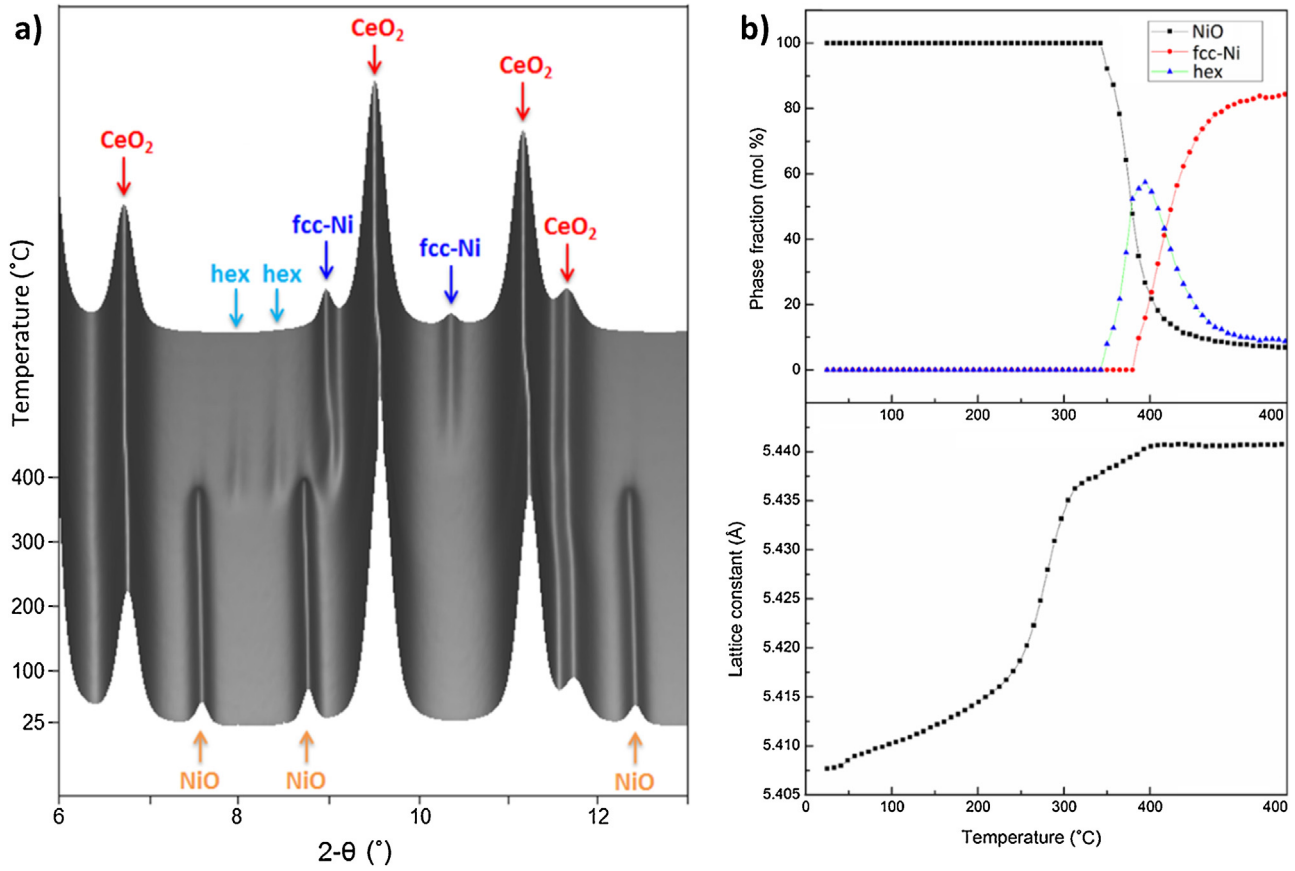

Fig. 2. (a) *In situ* XRD profiles of Ni/CeO_2 during the temperature-programmed reduction of Ni/CeO_2 in pure EtOH vapor, (b) Phase evolution of NiO to metallic Ni (the upper panel) and the change of Lattice constant of CeO_2 (the lower panel). Taken from Ref. [58]. Copyright 2013 by the American Chemical Society.

tion of alkali promoters, can also have a positive effect on reactivity [10,22,38–40].

Several groups have focused their attention on ESR catalysts which combine Ni and CeO_2 [21,41–56]. It has been established that these non-expensive systems are active for the ESR reaction [1,3]. Different approaches have been used to increase the interaction of Ni with CeO_2 [21,33,46] or to improve the performance of the ceria by mixing it with other oxides (ZrO_2, Al_2O_3, MgO, TiO_2, La_2O_3) [20,47,52–56]. Studies have been performed using well-defined or model catalysts, Ni-CeO_2(111) surfaces, and high-surface area powders which can be used in technical or industrial applications [33,42,57–59]. The morphology of the catalysts

have been examined with transmission electron microscopy (TEM) and scanning tunneling microscopy (STM) [50,58,60–62], while the catalyst compositions and the associated surface chemistry under reaction conditions have been investigated with in-situ techniques including ambient-pressure X-ray photoelectron spectroscopy (AP-XPS), time-resolved X-ray diffraction (TR-XRD), X-ray absorption fine structure (XAFS), and *in situ* diffuse reflectance infrared fourier transformed spectroscopy (DRIFTS) [33,44,58,62,63].

Insights from these studies have helped to establish the important role of ceria in the ESR process and in the development of strategies to facilitate catalytic conversion. We present these works below and discuss the importance of systematic studies using advanced characterization methods to deal with multi-components catalyst system. The article is organized as follows: First, studies focused in the behavior of powder catalysts will be presented, paying particular attention to the *in-situ* characterization of the catalyst active phase and its possible deactivation by carbon deposition. This will be followed by a discussion of works with model catalysts which examine the nature of the Ni-ceria interactions and the surface chemistry associated with the ESR process. The article ends with a description of approaches useful to favor metal-support interactions and enhance catalytic activity and selectivity.

2. Studies with Ni-CeO_2 powder catalysts

2.1. Catalytic activity, selectivity and phase evolution

Catalyst which contain Ni and ceria, or a combination of ceria and another oxide (Fig. 1 [45]), are active, selective and stable for the ESR reaction. In an earlier work it was shown that the Ni-ceria system is a non-expensive catalyst with a superior performance with respect to noble-metal based catalysts such as Rh/CeO_2 [33]. The synthesis of the catalyst led to a NiO-CeO_2 precursor that transformed under reaction conditions or after exposure to pure ethanol [58].

Fig. 2a shows recorded *in situ* XRD profiles for temperature programmed reduction of NiO/CeO_2 by ethanol [58]. The NiO phase present in the as-prepared sample is intact till 623 K, at which temperature it starts to be reduced to an intermediate hexagonal phase that further transforms into an fcc-Ni (face-centered cubic) phase. The intermediate phase is probably Ni_3C [64–67]. Quantification of the three Ni-related phases as a function of temperature is plotted in the upper panel of Fig. 2b. The fcc-Ni appears at 653 K and dominates at the end of the experiment. In addition to the reduction of NiO to Ni, the ceria reduction also occurs as evident by the lattice expansion of the CeO_2 in the lower panel of Fig. 2b. It is clear that the lattice expansion rate experiences a sharp increase from 503 to 573 K. This non-thermal expansion is regarded as evidence of partial reduction of Ce(IV) to Ce(III) with removal of oxygen atoms from the crystal structure [33,41]. This partial reduction of ceria occurs about 100 K prior to the reduction of NiO.

The catalytic activity of Ni-CeO_2 for ethanol steam reforming was tested at a constant EtOH/H_2O ratio of 1/8 with stepwise heating to 573, 623, 673 and 723 K. Many studies have indicated that a water to ethanol ratio higher than the stoichiometry ratio (i.e. 3:1) could inhibit coke formation [1,29,31]. Fig. 3 shows the phase evolution results derived from XRD and the mass spectroscopic results for the corresponding reaction products [58]. Rietveld refinement of the upper panel indicates that the NiO phase is directly reduced to the fcc-Ni phase at 623 K without forming the hexagonal phase as seen in the TPR reaction with ethanol (Fig. 2). Once the metallic Ni forms at 623 K, one can see the simultaneous formation of CO_2 and H_2, as expected for $C_2H_5OH + 3H_2O \leftrightarrow 6H_2 + 2CO_2$, indicating the cleavage of C—H and C—C bonds of ethanol by Ni. The signal

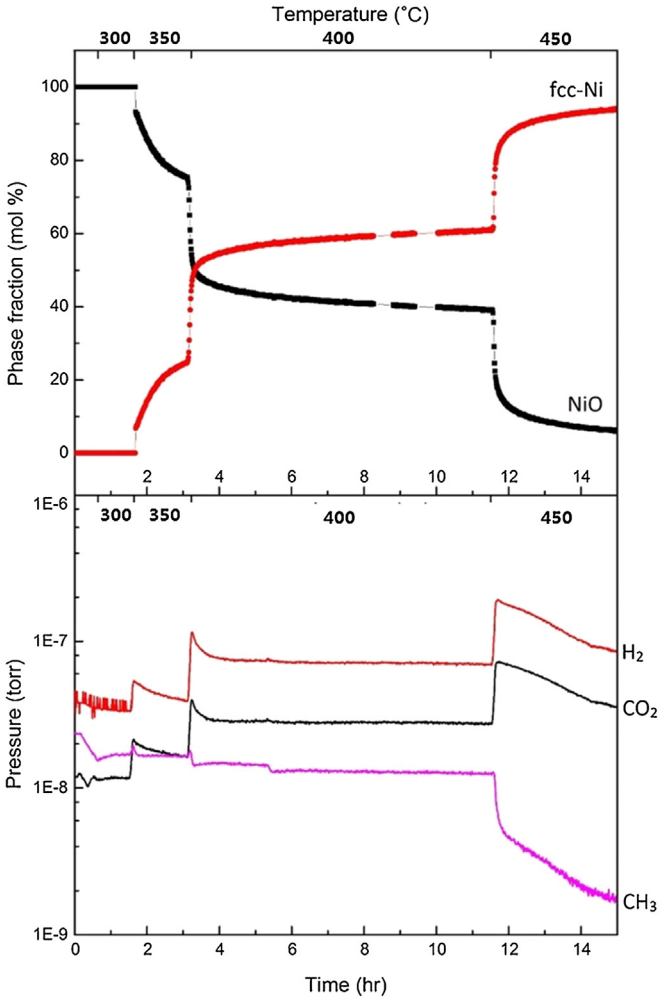

Fig. 3. Phase evolution of NiO to metallic Ni (the upper panel) derived from *in situ* XRD and the mass spectroscopic data of the residual gas (the lower panel) plotted with time and temperature for the steam reforming reaction with the EtOH/H_2O ratio at 1/8. Taken from Ref. [58]. Copyright 2013 by the American Chemical Society.

for CH_3 ($m/z = 15$) is the cracking fragment that could come either from ethanol or methane in the mass spectrometer. At temperatures above 673 K, it decreases constantly due to the consumption of ethanol and it implies that no significant amount of methane is formed. Note that the fraction of metallic Ni increases from 0 to 24% during the stay at 623 K, while the H_2 production peaks at the beginning of the NiO reduction then decreases with time. So it is the initial reduction that occurs at the surface of NiO particles that creates the active metal sites. At 623 K, the activity initially increases, and then remains stable for at least 9 h. At 723 K, over 85% of NiO is reduced. However, despite an initial boost of activity, all mass products start to decrease as a result of coke formation, which led to the clogging of reaction quartz tube (Fig. 3 lower panel). The deactivation process was reversible as the catalysts were reactivated once the deposited coke was removed by reaction with O_2 [58].

2.2. Reaction intermediates

The reaction intermediates on Ni/CeO_2, CeO_2 and NiO catalysts were investigated by *in situ* DRIFTS under steam reforming conditions (EtOH/H_2O = 1/8), as shown in Fig. 4 [58]. For the Ni/CeO_2 sample in Fig. 4a, the initial surface contains adsorbed water that contributes to a broad hump at 3000–3600 cm^{-1} and an OH scissoring band at 1650 cm^{-1} [62,68]. Also identified are the formed

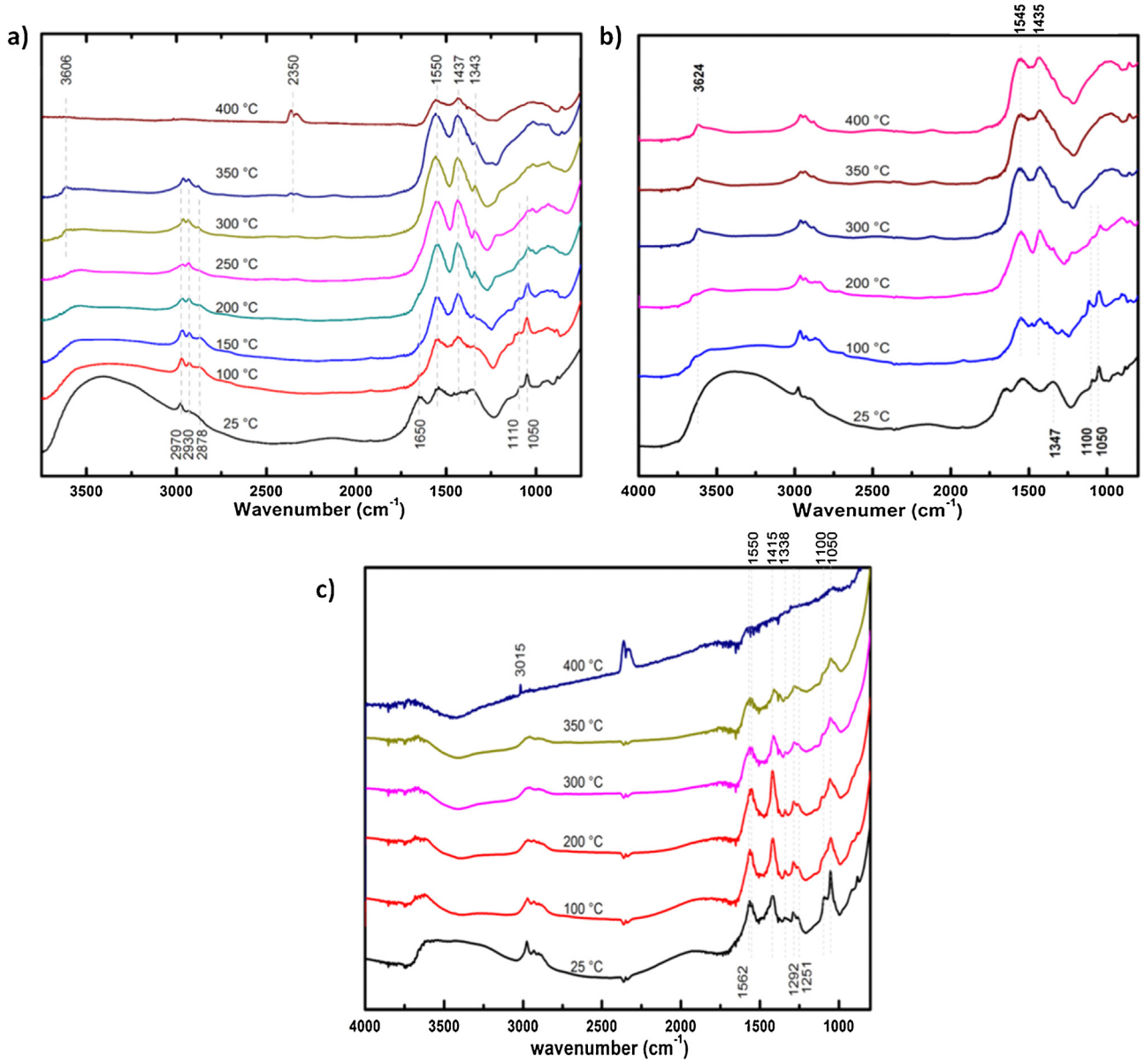

Fig. 4. DRIFTS spectra for (a) Ni/CeO_2, (b) bare CeO_2 and (c) bare NiO at elevating temperatures under steam reforming conditions. Taken from Ref. [58]. Copyright 2013 by the American Chemical Society.

ethoxy species with CH_n stretching bands in the region from 2800 to 3000 cm^{-1}, CO bands at 1110 and 1050 cm^{-1} [62,69]. At 373 K, the water-related bands diminish and more bands characteristic of acetate appear, including features at 1550 cm^{-1}, 1437 cm^{-1} and 1343 cm^{-1} for υ_{as}(COO), υ_s(COO) and $\delta(CH_3)$, respectively [70–72]. From 423 to 473 K, the ethoxy-related bands largely decrease in intensity, while the acetate-related band intensities increase. From 573 to 623 K, the CH_3 bending band of the acetate at 1343 cm^{-1} slightly decreases in intensity, which probably indicates the further oxidation of acetates species to carbonate as CO_2 gas phase (centered at 2350 cm^{-1}) is observed. At 673 K, the acetates/carbonates vigorously decompose to form CO_2, shown as a substantial drop of the COO bands (1550 and 1437 cm^{-1}) in accompany with a great increase of the CO_2 gas phase intensity as well as the disappearance of CH_3 bending band (1343 cm^{-1}) and the CH_n stretching band (2800–3000 cm^{-1}) from the acetate. An OH stretching band at 3606 cm^{-1} also disappears, which indicates that the hydroxyls are rapidly consumed at 673 K.

In the case where only CeO_2 is present under a steam reforming environment, shown in Fig. 4b, ethoxy and acetate are also observed at 298 K. Increasing the temperature to 573 K oxidizes the ethoxy to acetate. However, no further transformations of surface species were observed with additional temperature increases. All the acetates species along with the formed hydroxyl groups are retained on the surface and no production of CO_2 was detected.

It is clear that CeO_2 by itself cannot effectively decompose acetate and that the Ni interplay is critical for the C—H and C—C bond breaking, which is proved in Fig. 4c for bulk NiO sample under steam reforming reaction. XRD has shown that the partial reduction of NiO occurs at above 623 K [58]. Different from the ceria containing sample in Fig. 4a and b, the formation of hydroxyl groups are not pronounced on bulk Ni/NiO, since ceria is prone to dissociate water [73]. More importantly, at 673 K, along with the production of H_2 and CO_2, a significant amount of methane is released, evidenced by the CH_4 gas band at 3015 cm^{-1}. This demonstrates that, without a CeO_2 support, Ni is capable of breaking C—H/ C—C bonds of ethanol

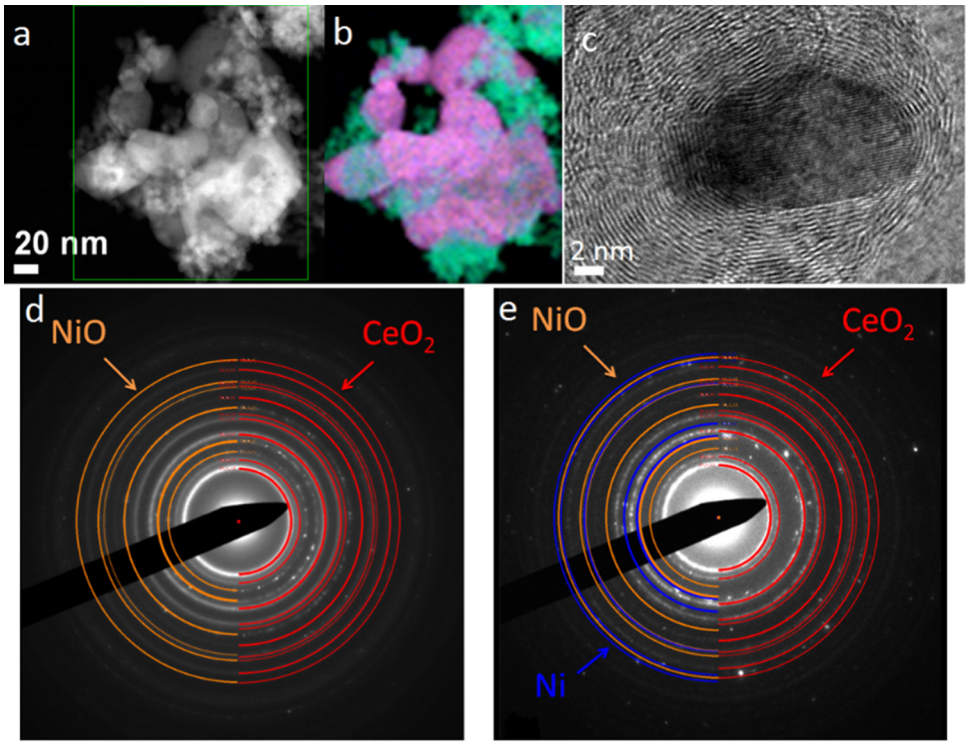

Fig. 5. Selected TEM, STEM, and ED images of the as-prepared Ni/CeO_2 (a, b, d) and after reduction in pure EtOH vapor (c, e). The EELS chemical map (b) is color coded to identify and indicate the presence of Ni (red), Ce (blue), and O (green). Taken from Ref. [58]. Copyright 2013 by the American Chemical Society. (For interpretation of the references to colour in this figure legend, the reader is referred to the web version of this article.)

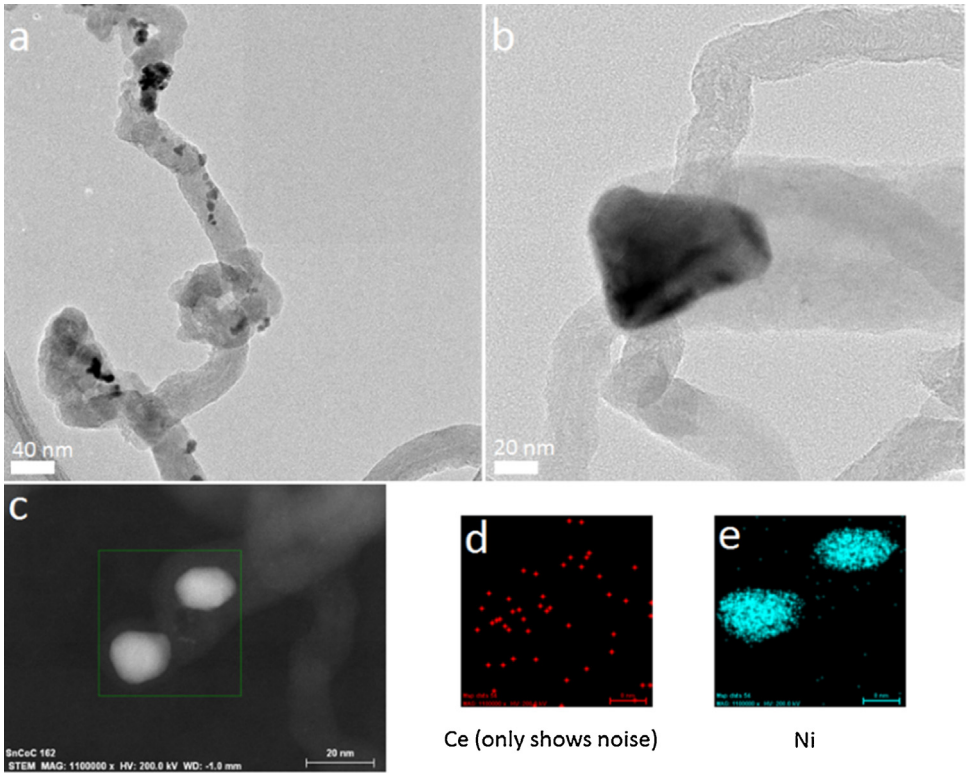

Fig. 6. Selected TEM and STEM collected after performing the steam reforming of ethanol on a Ni/CeO_2 catalyst showing the carbon fibers. Taken from Ref. [58]. Copyright 2013 by the American Chemical Society.

but it also leads the reforming reaction to an unselective pathway, where methanation take places [58].

Therefore, the reaction intermediates observed in Fig. 4a and c include ethoxy, acetate, carbonate and hydroxyl groups, the same species also observed in other systems like Co and Pt [27,62,69,74,75]. The role of each component of the Ni/CeO_2 catalyst in the reaction can be interpreted as: Ni is responsible for cleaving C—H/ C—C bonds of acetates or ethoxies, while the CeO_2 support, in addition to disperse NiO particles, has two functions: (1) facilitate the further oxidation of ethoxy species to acetates; (2) generate surface OH groups that promote the production of H_2 and CO_2 while inhibit the formation of CH_4 [58].

2.3. Deactivation and C-formation

The generation of surface carbon has been observed in studies for Ni-based catalysts [49,76–78]. The general routes for surface carbon deposition include [1]:

$$CH_n \rightarrow C + nH;$$

$$2CO \rightarrow C + CO_2;$$

$$nC_2H_4 \rightarrow \text{polymer} \rightarrow C.$$

Since ethylene is not observed in this study, the dehydrogenation of CH_n and Boudouard reaction are the two possible routes for the carbon formation on the Ni catalysts [57,58]. Considering the small amount of methane production on Ni/CeO_2, the CH_n groups from ethoxy and acetates species ultimately goes to H_2 and C instead of CH_4 [58]. Therefore, it is reasonable to pinpoint the methyl groups from the decomposition of acetates and ethoxy species are the major precursor for the carbon deposition on the surface of Ni/CeO_2 catalysts. Figs. 5 and 6 show the TEM images of the Ni/CeO_2 catalysts resulting from ethanol TPR and the ethanol steam reforming reaction, respectively. The sample reduced in pure EtOH vapor contains particles encased in layers of graphitic carbon (Fig. 5c), and electron diffraction (Fig. 5e) and Electron Energy Loss Spectroscopy (EELS) suggest the particles encased in graphitic carbon are mainly Ni or NiO.

In the sample after steam reforming (Fig. 6), particles are mostly supported on carbon fibers, and elemental analysis shows the particles on the tip contain only Ni without Ce (Fig. 6c–e). This indicates that these particles may have catalyzed the growth of the fiber (Fig. 6b) [79]. The fact that only graphitic carbon layers are present in the sample reduced in pure EtOH indicates the importance of H_2O for its mode of growth [58,80]. Filamentous carbon may not deactivate the catalyst as the encapsulating carbon does [77].

4. Studies with $Ni\text{-}CeO_2(111)$ and $Ni\text{-}CeO_{2\text{-}x}(111)$ model catalysts

Fundamental investigations of the reaction of ethanol on plain surfaces of Ni(111) [81,82], Ni(100) [83,84] and $CeO_2(111)$ [85] have been reported. To provide more insights on the $Ni\text{-}CeO_2$ interaction and its effects on the activity and selectivity of the reforming reaction, the properties of Ni nanoparticles supported on oxidized $CeO_2(111)$ and reduced $CeO_{2\text{-}x}(111)$ surfaces, designated as $Ni\text{-}CeO_2(111)$ and $Ni\text{-}CeO_{2\text{-}x}(111)$, were investigated.

4.1. Growth, morphology and chemical state of Ni on a $CeO_2(111)$ film

At a coverage of ~0.13 monolayer (ML), Ni forms two-dimensional particles with an average height of 0.3 nm on a CeO_2 film at 300 K as shown in the scanning tunneling microscopy (STM) images of Fig. 7 [57]. After heating to 700 K, Ni sinters into larger particles that are 2.7 nm wide and 0.5 nm high at the cost of particle density [57,60]. Fig. 8a depicts Ce 3d and Ni 2p XPS data collected upon deposition of Ni ($\theta < 0.4$ML) on $CeO_2(111)$ at room temperature followed by incremental annealing to 500, 700 and 800 K [37]. Ni predominantly remains metallic at 300 K with Ni $2p_{3/2}$ peak close to 853 eV. Heating the surface to 700–800 K causes extensive Ni oxidation to NiO (~854 eV), while mild reduction of ceria is observed. On the other hand, annealing to higher temperature also causes drastic changes in the line-shape of valence band features as shown in Fig. 8b [37]. The metallic Ni produces features in the region between 0 and 3 eV at 300 K for the occupied Ni 3d states [86,87]. Upon annealing, XPS data in Fig. 8a indicate the partial reduction of ceria and co-existence of Ni-NiO, but the valence UPS data show that the interaction of metallic Ni with the oxidize substrate significant reduce the density of occupied Ni 3d states near the Femi level, suggesting that the Ni is electronically perturbed with respect to bulk Ni [37,86,87]. This provides further evidence for the existence of strong metal-support interaction for small amounts of Ni on ceria [35,37,60].

4.2. Water dissociation on $Ni\text{-}CeO_2(111)$ and $Ni\text{-}CeO_{2\text{-}x}(111)$ surfaces

The dissociative chemisorption of water on the $Ni\text{-}CeO_2$ catalyst can be an important reaction step affecting its performance in the ESR process [33,36,57]. Fig. 9 shows the reaction of water with bare $CeO_2(111)$ and on a $Ni\text{-}CeO_2(111)$ film ($\theta_{Ni} < 0.15$ML, main oxidation state Ni^{2+}) studied by ambient-pressure X-ray photoelectron spectroscopy (AP-XPS) [36]. At 300 K, one can see clear peaks for gaseous H_2O, chemisorbed H_2O, adsorbed OH groups, and O from the lattice of ceria. After curve-fitting the O 1s spectra, one finds that annealing from 300 to 500 K led to the almost disappearance of the signal for chemisorbed H_2O and a substantial fraction of the adsorbed OH groups were also removed from the surface. Moreover, the amount of OH present on $Ni/CeO_2(111)$ at 500 K (0.37ML) was substantially larger than on $CeO_2(111)$ (0.20ML) [36]. This larger coverage of OH should facilitate the ESR reactions. The OH groups can easily react with CO and CH_n fragments to yield CO_2 and H_2 [33,37,57]. Furthermore, the heavy reduction of the ceria substrate lead to the generation of $Ni\text{-}CeO_{2\text{-}x}(111)$ systems that were quite active for the dissociation of water.

4.3. Ethanol reaction on $Ni\text{-}CeO_{2\text{-}x}(111)$ surfaces—adsorbates and surface state

After deposition, most of the Ni ($\theta_{Ni} < 0.2$ML) was oxidized as Ni^{2+} on the stoichiometric CeO_2 surface while significant amount of Ni still remained metallic on the reduced ceria surface [37,57,60]. XPS spectra indicate that ~80% and ~10% of the Ni nanoparticles present metallic on reduced ($CeO_{1.8}(111)$) and fully oxidized ceria ($CeO_2(111)$), respectively [57]. No significant changes of the oxidation states of Ni were observed on either surfaces after the surfaces were reacted with 2 L of ethanol at 700 K, and only ~8% of the ceria is further reduced to Ce^{3+} in the $Ni\text{-}CeO_{1.8}$ system. The sustained oxidation states of Ni reinforces the existence of a strong metal-oxide interaction between Ni and ceria, so that Ni^{2+} is not easily reduced by a 2 L ethanol exposure.

The surface chemistry of ethanol was studied on the $Ni\text{-}CeO_2$ and $Ni\text{-}CeO_{1.8}$ surfaces. No ethanol C—C bond activation was observed on the $Ni\text{-}CeO_2$ surface since most of the Ni remained as NiO during the reaction, in agreement with the powder system study which implies that metallic Ni is the active phase for C—C bond cleavage [57,58]. In contrast, ethanol activation was observed on the $Ni\text{-}CeO_{1.8}$ surface containing both Ni° and Ce^{3+} as shown by C 1s XPS data in Fig. 10a [57]. In addition to the two peaks for the

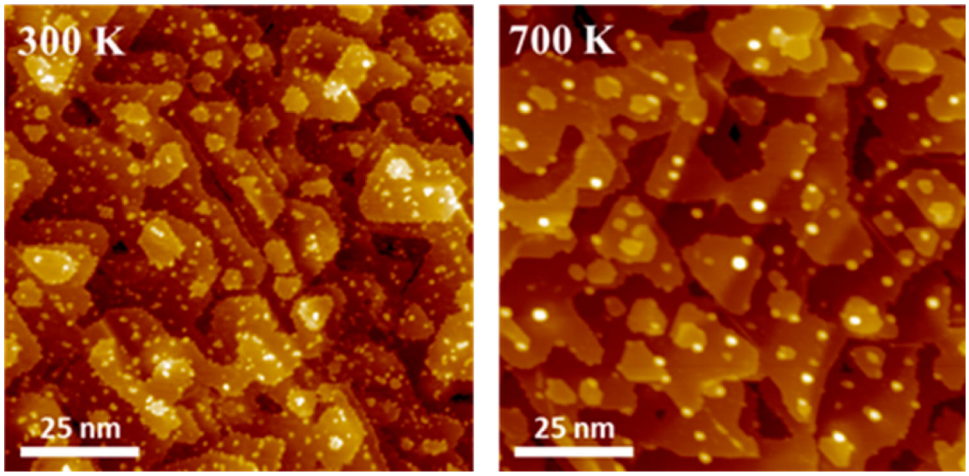

Fig. 7. STM images of 0.13ML Ni deposited on to $CeO_2(111)$ film at 300 K and after heating to 700 K, respectively. The image size is $100 \times 100\,nm^2$. Taken from Ref. [57]. Copyright 2015 by the American Chemical Society.

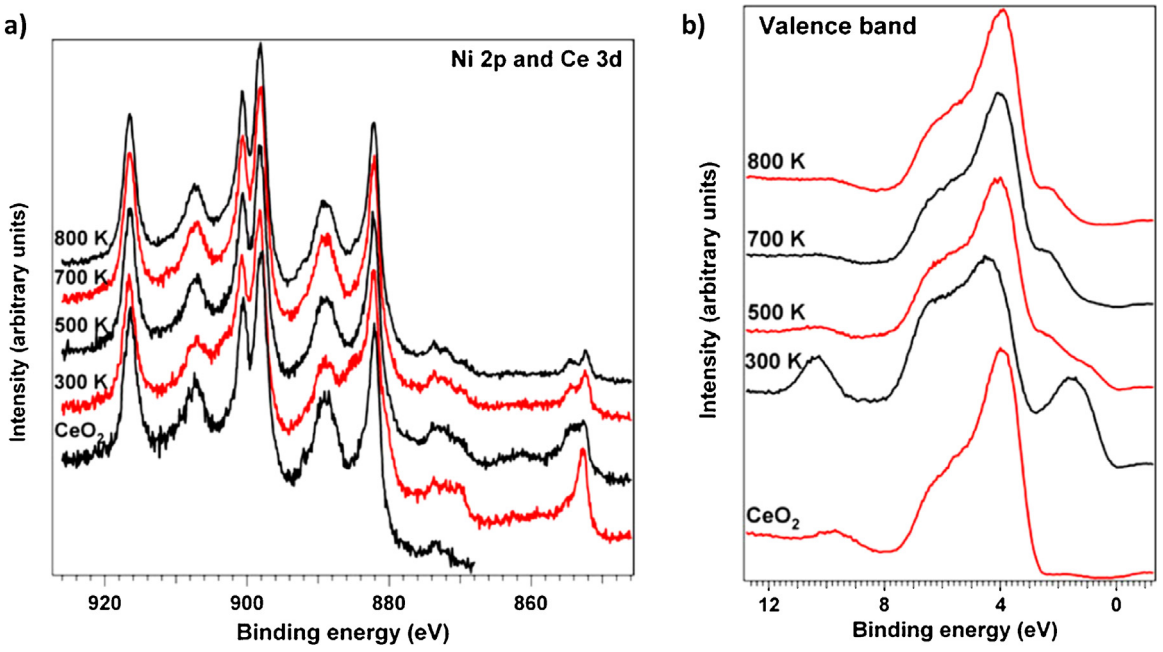

Fig. 8. (a) Evolution of the Ce 3d and Ni 2p photoemission lines as a function of the annealing temperature measured using a Mg Ka source (1253.6 eV). (b) He II (40.8 eV) excited valence band photoemission spectra for the Ni-$CeO_2(111)$ system as a function of the annealing temperature. Taken from Ref. [37]. Copyright 2011 by Springer.

ethoxy species (286.6 eV and 287.6 eV for methyl C and methoxy C, respectively), a new feature at 283.2 eV appears and it gradually increases in intensity upon heating up to 500 K. This peak can be assigned to the carbidic carbon of a Ni_3C species formed on the surface [88,89]. Nickel carbide was similarly observed in the study of other hydrocarbon related species on Ni [66,89–92]. As the carbide feature is developing, the ethoxy species are attenuated in parallel and eventually disappear at 500 K. This transformation is a strong indication of the C—C bond cleavage of the ethoxy species, which is not observed on the fully oxidized Ni-$CeO_2(111)$ and can be attributed to Ni-Ce^{3+} interactions [57]. A further increase of the temperature to 600 K induces a second transformation from carbide carbon (283.2 eV) to coke (C°, 284.5 eV), as Ni_3C is metastable and it decomposes to metallic Ni and surface carbon at elevated temperature [93]. This implicates that the coke formation probably goes through nickel carbide as an intermediate phase [57]. By 700 K, a significant amount of coke with a minor amounts of Ni_3C is still seen on the surface, although there is a minor decrease in intensity of the coke/Ni_3C features, suggesting a limited capability for coke removal from the surface under these conditions.

The ethanol reaction on Ni-$CeO_{1.8}(111)$ was also studied in the presence of background water. 2L of ethanol were initially dosed onto the Ni-$CeO_{1.8}(111)$ surface at 300 K, then the sample was heated to 400, 500, 600 and 700 K under a background of 2×10^{-8} Torr of water, as shown in Fig. 10b. The evolution from ethoxy species to Ni_3C/coke emerged similarly to the one shown in Fig. 10a. However, further increasing the temperature to 700 K led to removal of all the carbon related species from the surface, leaving the surface free of coke. This implicates that the presence of water and/or OH groups not only completes the catalytic cycle in the steam reforming of ethanol to produce more hydrogen product, but it is also crucial to prevent the formation of coke through oxidation of the surface carbon at higher temperature (>700 K),

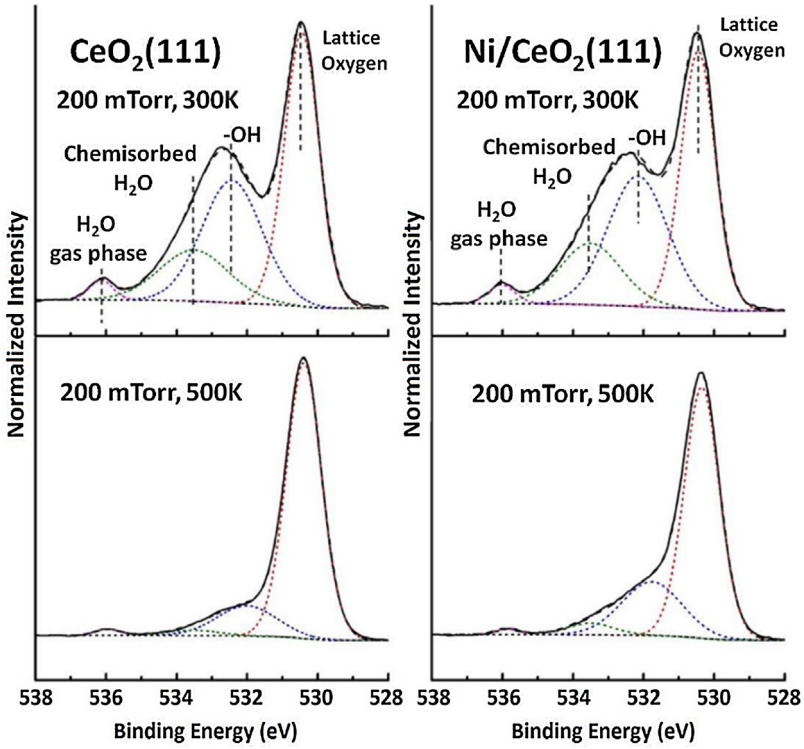

Fig. 9. O 1s XPS spectra for CeO_2(111) and Ni/CeO_2(111) under 200 mTorr of water at 300 and 500 K. The coverage of Ni in Ni/CeO_2(111) was ~0.15ML. Taken from Ref. [36]. Copyright 2015 by Wiley.

which will be further proved by analyzing the desorbed products.

4.4. Ethanol reaction on Ni-CeO_{2-x}(111) surfaces—desorption of products

TPD results with/without water are displayed in Fig. 11. In order to match the XPS experiments, we performed the TPD studies with a dose of 2 L of ethanol alone (black line) and with 2 L of ethanol under 2×10^{-8} Torr of D_2O vapor in the background (red line). First, following the ethanol TPD without D_2O, three distinguishable peaks for CO are observed with desorption temperatures at 346, 500 and 596 K. The CO produced at 346 K here is attributed to the decarbonylation of the methylene C (—CH_2 —O—) in the ethoxy species adsorbed on metallic Ni [81]. The remaining two CO desorption peaks with a temperature threshold at 500 and 596 K were not observed in a previous study of ethanol on a plain Ni film [81,94], suggesting that they are associated with the ceria substrate and interfaces formed with Ni. Also note that the reported temperature regime for CO desorption from a Ni film is below 450 K [95–97]. These two higher temperature peaks are therefore reaction-limited. As shown in Fig. 10a, at 500 K, only Ni_3C and coke remain on the surface, no hydrocarbon related species are evident in the C 1s, and coincident with the CO evolution at a 500 K temperature threshold, H_2 is also produced in the TPD data. These results all imply that the CO peak at 500 K likely originated from ethoxy species on ceria sites that diffused to the metal and further decarbonylated [57].

The oxidation of the surface Ni_3C/C requires oxygen transfer from the ceria substrate to the Ni nanoparticles via the reduction of ceria. This process is only favored at higher temperatures [57]. Hence, the observation of the CO peak at 596 K could be attributed to the surface Ni_3C/C on Ni nanoparticles combining with the O transferred from the support ceria oxides. Additionally, no CO_2 production was detected and negligible CH_4 was produced at ~500 K (not shown here), indicating that the coke formation was mainly due to the dehydrogenation of the surface methyl groups instead of the Boudouard reaction [57]. The possible reaction routes for the desorption profiles in Fig. 11 in the absence of water are proposed as follows:

$$CH_3CH_2OH(ad) \rightarrow CH_3CH_2O{-}(ad) + {-}H(ad), \quad 300\,K \tag{1}$$

$$\text{On Ni sites}: CH_3CH_2O{-} \rightarrow CH_3{-}(ad) + CO(g) + 2{-}H(ad), \quad 300\text{–}450\,K; \tag{2}$$

$$CH_3(ad) \rightarrow C(coke) + 3{-}H(ad),\ 300\text{–}450\,K;$$

$$2\text{-}H(ad) \rightarrow H_2(g),\ 300\text{–}450\,K;$$

$$\text{On ceria sites}: CH_3CH_2O{-} \rightarrow CH_3CHO(ad) + {-}H(ad) \quad \sim 500\,K; \tag{3}$$

$$\text{Then diffuse to Ni sites}: CH_3CHO(ad) \rightarrow CH_3(ad) + CO(g) + {-}H(ad),\ \sim 500\,K;$$

$$-O(lattice) + Ni_3C/C \rightarrow Ni^0 + CO(g),\ > 600\,K;$$

To study the effects of hydroxyl groups on the ethanol reaction, ethanol TPD under D_2O vapor pressure (2×10^{-8} Torr) over Ni-$CeO_{1.8}$ is presented as red lines in Fig. 11. D_2O was used here to distinguish the hydrogen from ethanol from that of water. The major difference is, at temperature above 500 K, D_2 and DH were

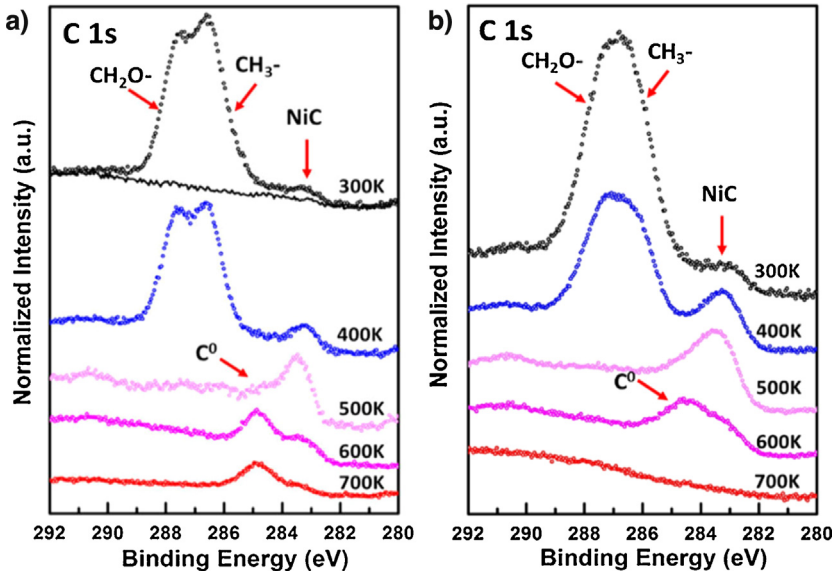

Fig. 10. C 1s spectra of 2 L ethanol dose on Ni-$CeO_{1.8}$(111) surface at 300 K followed by heating up to 400, 500, 600, and 700 K: (a) heating in UHV (b) heating under a background of 2×10^{-8} Torr pressure of water. Reproduced from Ref. [57]. Copyright 2015 by the American Chemical Society.

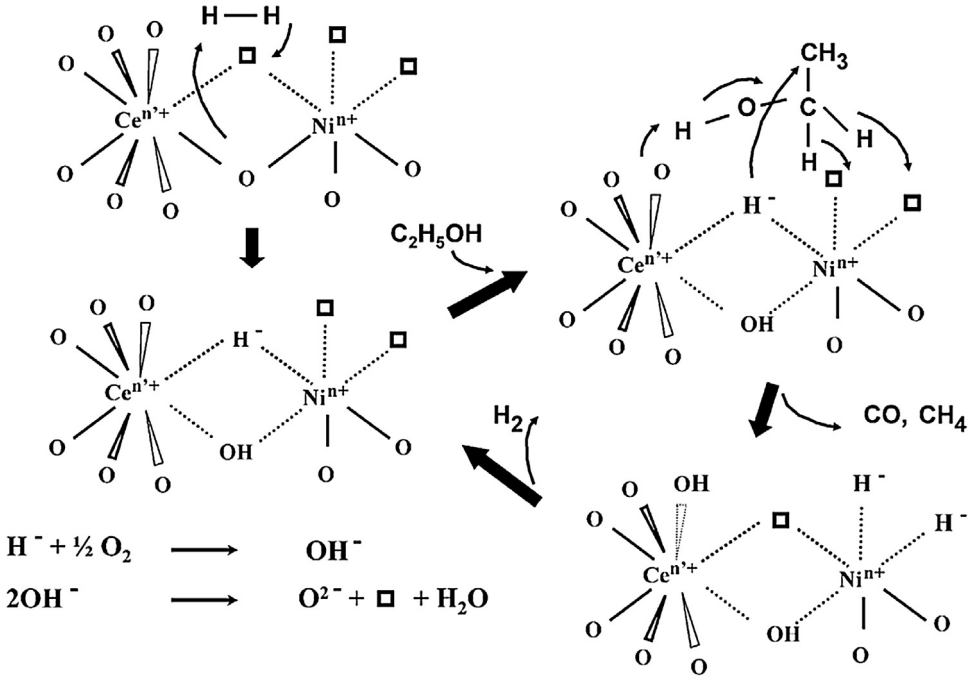

Scheme 1. Mechanism and active-site modeling for ethanol transformation over $CeNiH_zO_y$ nano-oxyhydride. (Ni^{n+}: Ni^{2+} or $Ni^{\delta+}$ and $Ce^{n'+}$: Ce^{4+} or Ce^{3+}) Taken from Ref. [46]. Copyright 2011 by Wiley.

detected in addition to the CO and H_2 production, indicating that D_2O has been involved in the reaction at this temperature. More importantly, for the CO evolution, the peak area of the 600 K CO peaks resulting from the oxidation of surface Ni_3C/coke are estimated to be 40% larger than those from the D_2O free surface. Considering the fact that the XPS data shows a coke free surface at 700 K in the C 1s spectra of Fig. 10b, and also noting that a significant amount of D_2 is produced from D_2O simultaneously at ~600 K due to the transfer of oxygen to ceria/Ni, one can draw the conclusion that the OD groups formed upon D_2O exposure can play a vital role here in assisting the removal of coke from the surface in the form of CO, which can be interpreted as follows:

$$D_2O(g) \rightarrow -OD(ad) + \text{-}D(ad), \quad (1)$$

$$-OD(ad) \rightarrow O(lattice) + \text{-}D(ad), > 600\,K; \quad (2)$$

$$-O(lattice) + Ni_3C/C \rightarrow Ni^0 + CO(g), > 600\,K; \quad (3)$$

$$Or -OD(ad) + Ni_3C/C \rightarrow Ni^0 + CO(g) + \text{-}D(ad), > 600\,K;$$

Our model surfaces studied here can have a strong correlation to steady state conditions of the ESR over powder samples, at temperatures above 600 K. It is likely that two competing processes will

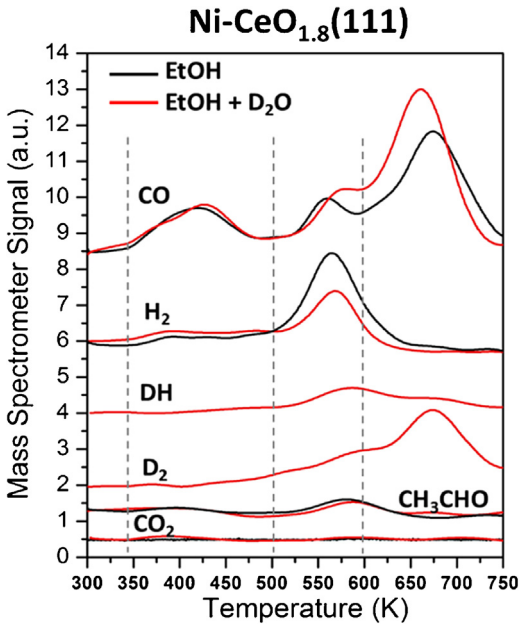

Fig. 11. TPD results from 2 L of ethanol adsorbed at 300 K on Ni-$CeO_{1.8}$(111) film: black line, temperature ramping without D_2O, redline, temperature ramping under 2×10^{-8} Torr D_2O background pressure. Taken from Ref. [57]. Copyright 2015 by the American Chemical Society. (For interpretation of the references to color in this figure legend, the reader is referred to the web version of this article.)

occur on the surface: the surface carbon accumulation and the oxidation of surface carbon by water/hydroxyls. The ability to sustain sites that can do both steps including C—C bond breaking and OH formation is critical and can now be joined with an additional step which includes the remediation of coke formation. The later process relies heavily on the redox nature of the oxide substrate as well as the metal-oxide interaction facilitating the oxygen transport.

5. Modifying Ni-Ce catalysts

5.1. *Protecting the Ni-Ce interaction in $Ce_{1-x}Ni_xO_{2-y}$ solid solution catalysts*

Based on the aforementioned studies, it was established that small Ni nanoparticles in close contact with the cerium oxide substrate exhibit strong metal-oxide interaction to produce active surface sites that are very important for the cleavage of C—C and C—H bonds and for subsequent formation of CO_2 and H_2 [33]. An effective approach to maintain strong Ni ↔ CeO_2 interactions involves the preparation of $Ce_{1-x}Ni_xO_{2-y}$ solid solutions [33,98]. The XRD data in the left panel of Fig. 12 shows that the solubility limit of Ce-Ni exchange in ceria is in the range of 10–12% whereas the remaining Ni segregated as NiO phase outside the ceria lattice. As the temperature increased, rietveld refinement revealed that NiO survived up to about 673 K under reaction conditions, and this temperature a NiO → Ni transformation occurred. The appearance of the metallic Ni phase correlated with a substantial increase in the production of H_2 in the right panel of Fig. 12. Thus, the activated $Ni_{0.2}Ce_{0.8}O_{2-y}$ catalysts contain a small amount of metallic Ni (particles less than 3 nm in diameter) dispersed on a nickel-doped ceria support [33]. The right panel of Fig. 12 also compares the hydrogen production of $Ce_{1-x}Ni_xO_{2-y}$ and a Rh-ceria catalyst. Clearly, at a temperature above 673 K, the $Ni_{0.2}Ce_{0.8}O_{2-y}$ catalyst shows a better hydrogen production activity and is stable over time [33]. In the case of $Ni_{0.1}Ce_{0.9}O_{2-y}$ sample, since no significant amount of Ni particles was detected by XRD and most of the Ni are embedded into ceria lattice [33,98], it exhibits a lower activity compared to $Ni_{0.2}Ce_{0.8}O_{2-y}$ at temperatures above 673 K. The calculated ethanol consumption of $Ni_{0.2}Ce_{0.8}O_{2-y}$ at 673 K was 100%, and the selectivity for H_2 formation was 67%. Furthermore, Rietveld refinement of the in situ XRD patterns showed that $Ni_{0.2}Ce_{0.8}O_{2-y}$ exhibits a ceria lattice expansion 1.5 times larger than the conventional impregnated Ni_{10}/CeO_2 catalysts at temperatures between 473 and 523 K, indicating the significant reduction of ceria during the steam reforming process [33]. This is because the doping of ceria with Ni induces strain in the oxide lattice and favors the formation of O vacancies [33,98]. A large concentration of O vacancies, and related defects, will in turn enhance the dispersion of reduced Ni on the oxide surface and facilitate the cleavage of the O—H bonds in water and ethanol [33].

Moreover, these defects related active sites also have been generated by Duhamel et al. by H_2 pretreatment of a similar Ni-ceria system [46,59,99,100]. As shown by the Inelastic Neutron Scattering (INS) spectrum in Fig. 13, two intense bands are observed at about 460 and 870 cm^{-1} after the pretreatment with H_2 at 523 K due to the insertion of different hydrogen species [99]. The peak at 460 cm^{-1} was assigned to the hydride species while the large band at 870 cm^{-1} was associated with hydrogen species interacting with metallic Ni [46,99,100]. Therefore, during the H_2 pretreatment, a

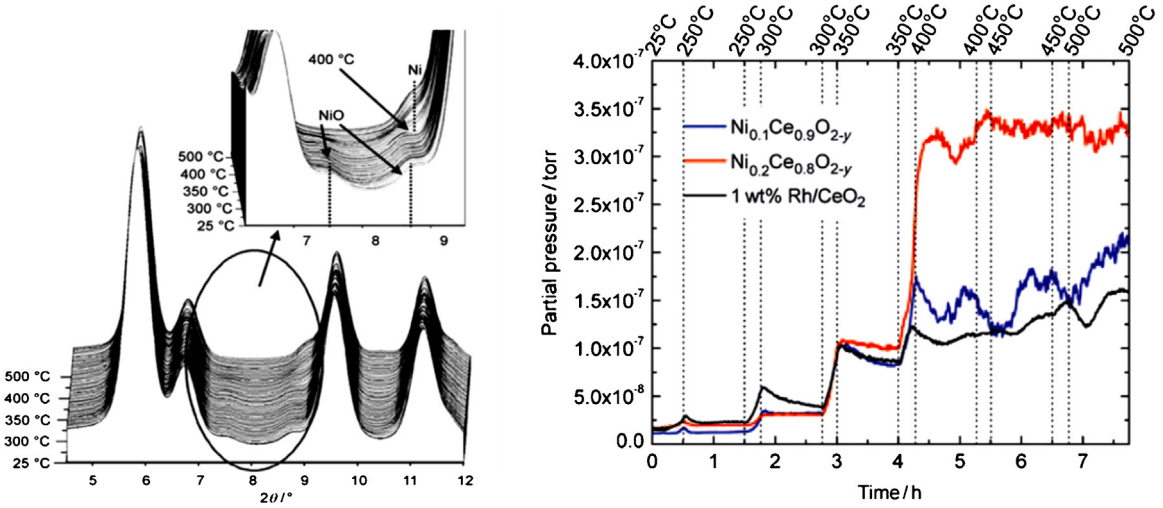

Fig. 12. Left: *in situ* X-ray diffraction pattern for $Ni_{0.2}Ce_{0.8}O_{2-y}$ collected during the ethanol steam reforming reaction. Right: Hydrogen production plots for ethanol steam reforming over $Ni_{0.1}Ce_{0.9}O_{2-y}$, $Ni_{0.2}Ce_{0.8}O_{2-y}$, and 1 wt% Rh/CeO_2. Taken from Ref. [33]. Copyright 2010 by Wiley.

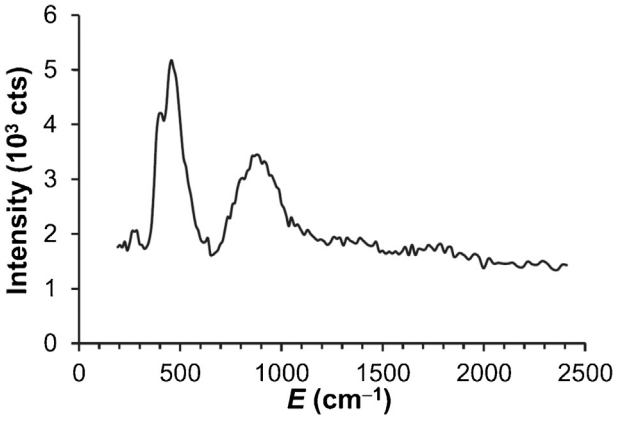

Fig. 13. INS spectrum of $CeNi_1O_y$ treated in H_2 at 523 K (250 °C) (after subtraction of the spectrum obtained on $CeNi_1O_y$ treated in vacuum at 473 K (200 °C). Taken from Ref. [99]. Copyright 2015 by Elsevier.

Ni-Ce mixed oxide transforms into an oxyhydride ($CeNi_XH_ZO_Y$) which could play an important role in the ESR reaction [46,99]. Evidence for the formation of a $CeNi_XH_ZO_Y$ compound has also been found in experiments of ambient-pressure XPS. Scheme 1 shows a mechanism for the formation of this oxyhydride and how this compound could be involved in the ESR process [46,99].

5.2. Addition of interfacial stabilizers: Ni-W-Ce and complex mixed-metal oxide catalysts

Several paths have been followed to enhance the interaction of Ni with CeO_2 [21,33,46] or to improve the performance of the ceria by mixing it with other oxides (ZrO_2, Al_2O_3, MgO, TiO_2, La_2O_3) [20,47,52–56]. Other than Ni, many other dopants including Zr [20,24,47,101–107], Tb [106–110], Ca [27,111,112], La [113–116] etc. have been employed aiming at enhancing the redox properties and thermal stability of pure ceria, which is the key for highly active and stable steam reforming of ethanol [1]. Significant catalytic improvements with respect to steam reforming of ethanol have been shown for the Ni based ceria catalysts with dopants [20,41,45,47,48]. Fig. 14 shows the impact of Zr-Ce ratio on the selectivity of ethanol steam reforming [48]. The samples with Zr doping exhibit better catalytic performance than the Ni supported on either pure ceria or ZrO_2 [48], and the highest selectivity of H_2/CO_2 was achieved when the molar ratio of Ce/Zr is 0.7 [48]. In a structural level, the catalytic enhancement could be illustrated by the XRD pattern of Ni-Ce-Zr catalysts with variable Ce/Zr ratio, as

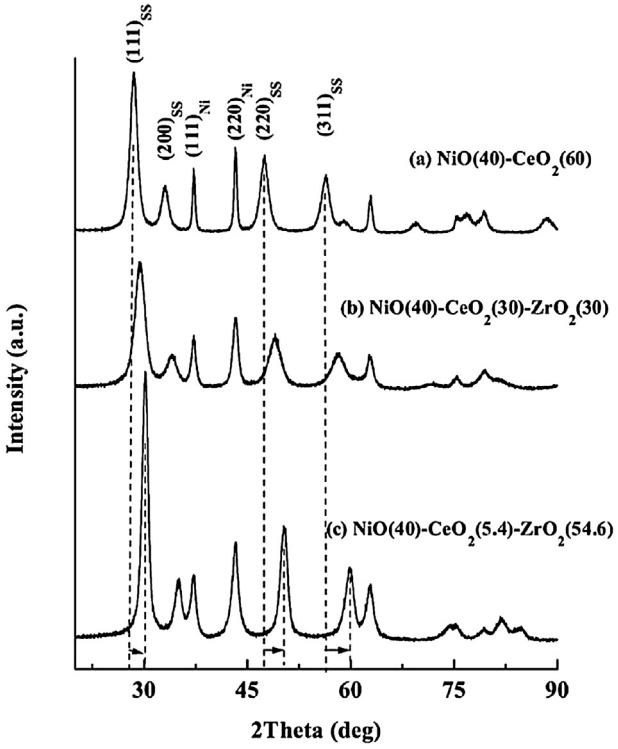

Fig. 15. XRD pattern of NiO-CeO_2-ZrO_2 catalysts, peaks corresponding to CeO_2-ZrO_2 solid solutions (SS) and NiO (Ni) are marked. Taken from Ref. [47]. Copyright 2003 by Elsevier.

shown in Fig. 15 [47]. The Ce-Zr solid solution unit cell parameter changes with the Ce/Zr ratio due to the smaller size of Zr^{4+} cations [47]. Also, when the eight-coordinated Ce^{4+} is substituted by a six-coordinated Zr^{4+} cation, defects centers are created. Furthermore, zirconia doping promotes the formation of Ce^{3+} since the smaller size of Zr^{4+} cations take part in removing the strain associated with the increase of ionic size accompanying the Ce^{4+} to Ce^{3+} transition [47]. As a result, the incorporation of Zr in ceria will retard the sintering of ceria crystallites, preserve the oxygen vacancies and facilitate the reduction of Ce^{4+} to Ce^{3+}, which are responsible for the superior oxygen storage capacity of Ce-Zr solid solution [47].

Motivated by this, we also investigated the Ni-W-Ce ternary catalyst for steam reforming of ethanol. W with a 6+ formal oxidation state and oxides with a crystal structure different from that of ceria can induce substantial electronic and structural pertur-

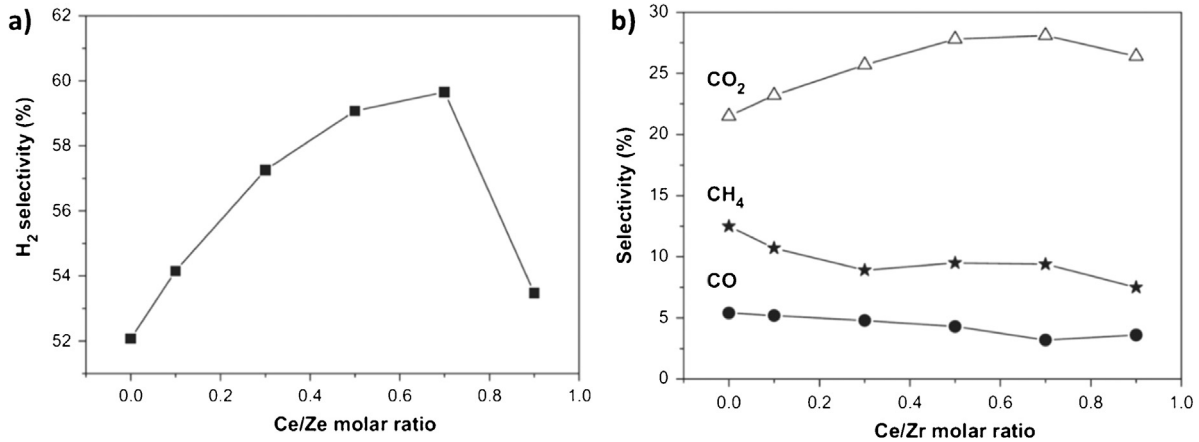

Fig. 14. Ethanol steam reforming selectivity over Ni/Zr-Ce-X catalysts (X = 0, 0.1, 0.3, 0.5, 0.7, and 0.9): (a) hydrogen selectivity, (b) CO, CO_2 and CH_4 selectivity. Reproduced from Ref. [48]. Copyright 2008 by Elsevier.

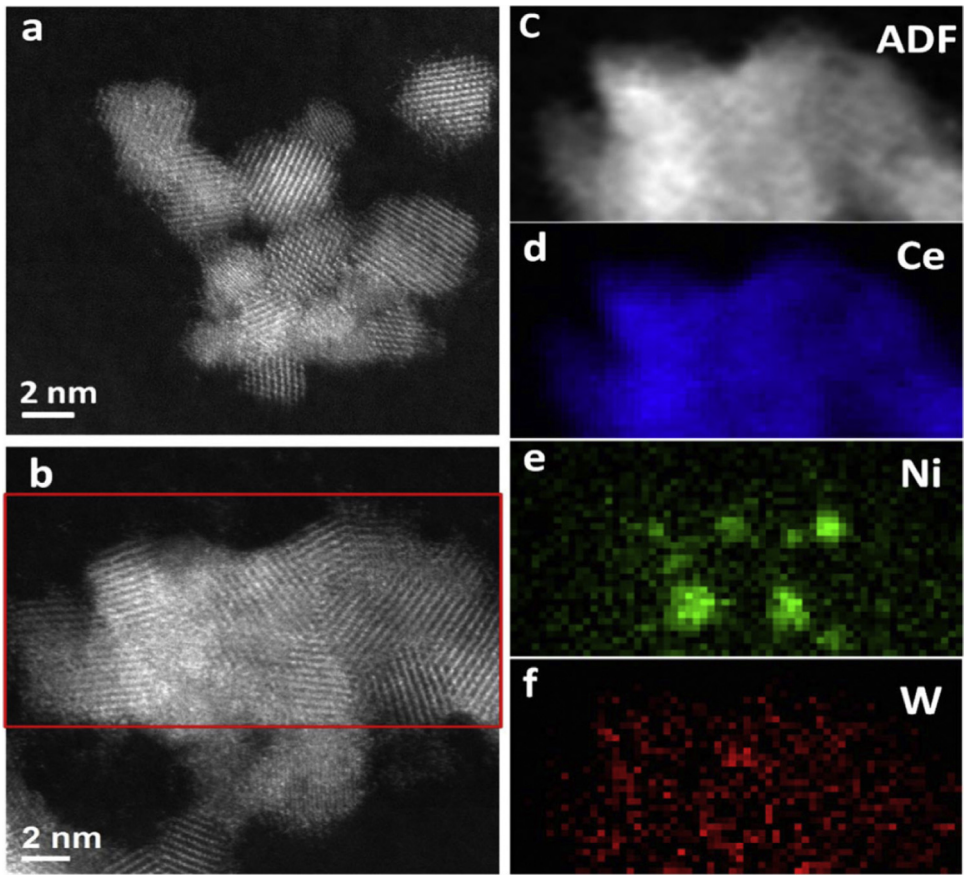

Fig. 16. Selected STEM images (a and b) and EELS mapping (c–f) of the as-prepared $Ni_{0.2}W_{0.1}Ce_{0.7}O_2$. The area inside the square displayed in Fig. 15b was used for the EELS mapping. The element map was colored to identify and indicate the distribution of corresponding elements: Ce (blue), Ni (green) and W (red). Taken from Ref. [44]. Copyright 2015 by Elsevier. (For interpretation of the references to color in this figure legend, the reader is referred to the web version of this article.)

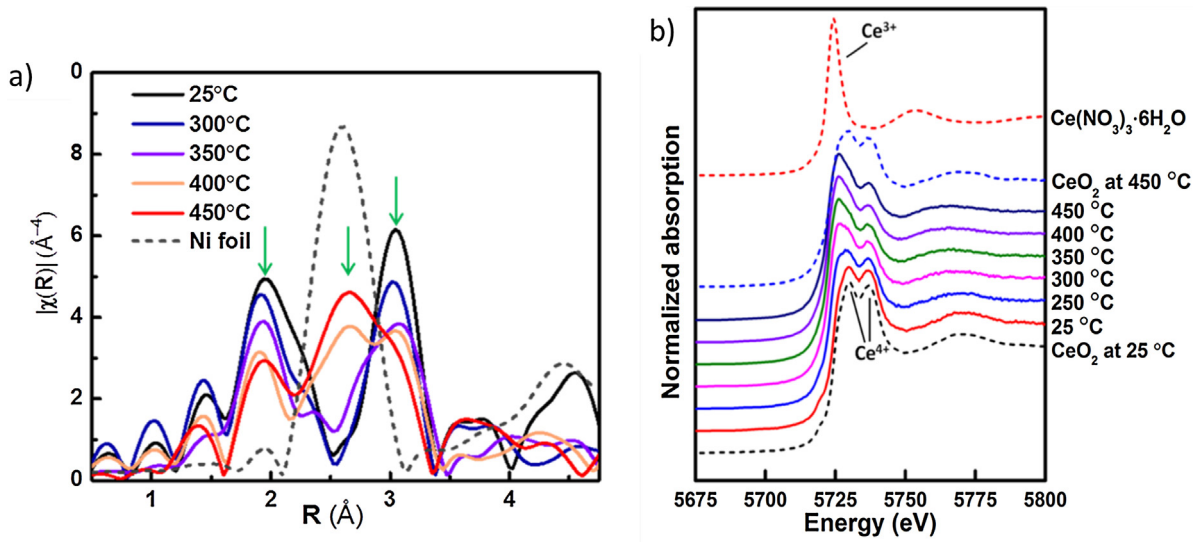

Fig. 17. (a) *In situ* Ni K-edge Fourier transformed R-space of EXAFS spectra and (b) *in situ* Ce L_3-edge XANES spectra collected over $Ni_{0.2}W_{0.1}Ce_{0.7}O_2$ during ethanol steam reforming reaction at elevated temperatures (solid line). Dash lines show the reference spectra as indicated. Taken from Ref. [44]. Copyright 2015 by Elsevier.

bations in the host oxide [44]. TEM images of the as-synthesized $Ni_{0.2}W_{0.1}Ce_{0.7}O_2$ sample are presented in Fig. 16 [44]. The ceria nanoparticles exhibited approximated sphere morphology with a size of 4–6 nm. Fig. 16b–f shows a scanning transmission electron microscopy (STEM) image of the sample and the corresponding electron energy loss spectroscopy (EELS) mapping of Ce, Ni and W. As Fig. 16d shows, all the particles presented in Fig. 16b were ceria nanoparticles, no big crystalline particles related to Ni or W were seen. In fact, Ni exhibited two forms of structures associated with the ceria lattice (Fig. 16e): small NiO clusters (<2 nm cluster size)

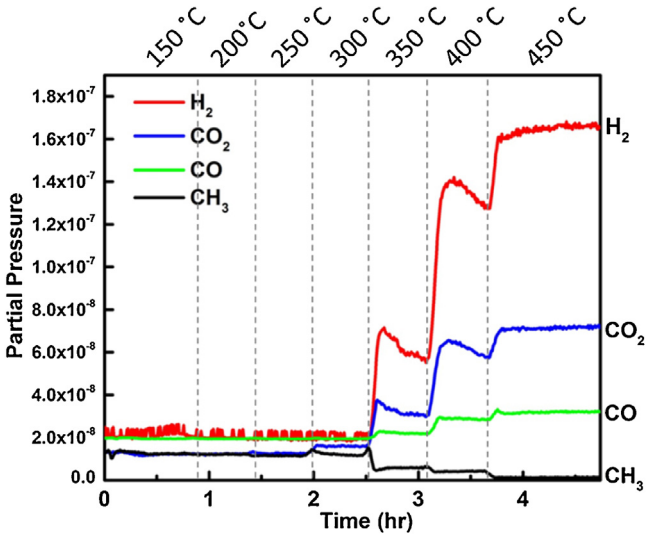

Fig. 18. Mass spectroscopic data of the reaction products (H_2, CO_2, CO and CH_4) during the ethanol steam reforming over a $Ni_{0.2}W_{0.1}Ce_{0.7}O_2$ catalyst. At 723 K (450 °C), the ethanol conversion on this catalyst was 100%. Taken from Ref. [44]. Copyright 2015 by Elsevier.

and mono dispersed Ni. In contrast, W was evenly distributed over all the imaged ceria particles without any aggregation in Fig. 16f. Further examination with XRD, XAFS and PDF experiments ascertains that for the as-prepared $Ni_{0.2}W_{0.1}Ce_{0.7}O_2$ catalysts [44], all the W and part of the Ni were incorporated into the CeO_2 lattice, with the remaining Ni forming highly dispersed nano NiO (<2 nm) outside the Ni-W-Ce oxide structure.

In situ XAFS experiments in Fig. 17 reveal the phase evolution of $Ni_{0.2}W_{0.1}Ce_{0.7}O_2$ catalyst under steam reforming conditions [44]. At 723 K in Fig. 17a, the metallic Ni–Ni peak has emerged and it is broad and of much lower intensity compared to the one for a Ni foil, which indicates that the newly formed metallic Ni phase is still present as small clusters (low coordination number) instead of forming large Ni particles [44]. On the other hand, in Fig. 17b, the extent of ceria reduction on the $Ni_{0.2}W_{0.1}Ce_{0.7}O_2$ catalyst is much severe than for the undoped ceria, indicating the formation of O vacancies (defects) [44]. Therefore, under reaction conditions, an extremely small particle size of Ni (or even atomic Ni) gave it a strong adherence to the ceria support with a substantial amount of defects, which guaranteed the sufficient supply of OH from the surrounding ceria and also prevented its sintering. As shown in Fig. 18, no decay of H_2 production and no observable production of methane was seen for the solid solution Ni samples at 723 K compared to the impregnated Ni/CeO_2 samples [44]. Furthermore, as proved in the XPS and UPS results in Fig. 8, small Ni particles in close contact with ceria are electronically perturbed [33,98] and do not exhibit the typical methanation activity of bulk nickel [35,98,117,118]. Big Ni particles will decompose ethanol into CH_n groups and C atoms [117,118]. As a consequence of this, carbon will be accumulated on the catalysts surface and finally will encapsulate the active sites.

6. Conclusions

The Ni-CeO_x system is an active and non-expensive catalyst for the steam reforming of ethanol, with a complex interplay between the active species (Ni and CeO_x) in the mechanistic pathways that lead to H_2 generation. Both powder and well-defined model systems have been studied extensively in an effort to identify critical aspects for this reaction. It has been established that the active state of the catalyst contains Ni° and Ce^{3+}, while the dissociation of H_2O and C—C, C—H bond breaking in ethanol are important steps in the process. Furthermore, it has been shown that NiC is likely to be a transition phase for carbon formation (coke) while hydroxyl groups formed on ceria by dissociating H_2O play a crucial role in the mitigation of surface carbon. In the Ni-ceria catalysts for ethanol steam reforming, the ceria plays two roles: First, it modifies the electronic properties of nickel tuning the metal chemical properties; And second, it participates directly in the ESR reaction helping with the cleavage of O—H bonds and preventing deactivation by coke deposition.

Acknowledgements

The research performed at Brookhaven National Laboratory was supported by the U.S. Department of Energy, Office of Science, Office of Basic Energy Sciences, and Catalysis Science Program under contract No. DE-SC0012704. This work used resources of the Center for Functional Nanomaterials (CFN-BNL) and the National Synchrotron Light Source (NSLS) which are DOE Office of Science User Facilities.

Appendix A. Supplementary data

Supplementary data associated with this article can be found, in the online version, at http://dx.doi.org/10.1016/j.apcatb.2016.03.013.

References

[1] L.V. Mattos, G. Jacobs, B.H. Davis, F.B. Noronha, Chem. Rev. 112 (2012) 4094–4123.
[2] P.R.d.l. Piscina, N. Homs, Chem. Soc. Rev. 37 (2008) 2459–2467.
[3] A. Haryanto, S. Fernando, N. Murali, S. Adhikari, Energy Fuels 19 (2005) 2098–2106.
[4] F. Frusteri, S. Freni, L. Spadaro, V. Chiodo, G. Bonura, S. Donato, S. Cavallaro, Catal. Commun. 5 (2004) 611–615.
[5] J. Llorca, N.s. Homs, J. Sales, P.Rr. de la Piscina, J. Catal. 209 (2002) 306–317.
[6] S. Cavallaro, Energy Fuels 14 (2000) 1195–1199.
[7] V.V. Galvita, G.L. Semin, V.D. Belyaev, V.A. Semikolenov, P. Tsiakaras, V.A. Sobyanin, Appl. Catal. A 220 (2001) 123–127.
[8] D.K. Liguras, D.I. Kondarides, X.E. Verykios, Appl. Catal. B 43 (2003) 345–354.
[9] A. Romero, M. Jobbágy, M. Laborde, G. Baronetti, N. Amadeo, Appl. Catal. A 470 (2014) 398–404.
[10] V. Palma, F. Castaldo, P. Ciambelli, G. Iaquaniello, Appl. Catal. B 145 (2014) 73–84.
[11] M.C. Sánchez-Sánchez, R.M. Navarro, J.L.G. Fierro, Int. J. Hydrogen Energy 32 (2007) 1462–1471.
[12] N. Homs, J. Llorca, P.R. de la Piscina, Catal. Today 116 (2006) 361–366.
[13] A.J. Vizcaíno, A. Carrero, J.A. Calles, Catal. Today 146 (2009) 63–70.
[14] A.L. Da Silva, J.P. Den Breejen, L.V. Mattos, J.H. Bitter, K.P. De Jong, F.B. Noronha, J. Catal. 318 (2014) 67–74.
[15] C.N. Ávila-Neto, D. Zanchet, C.E. Hori, R.U. Ribeiro, J.M.C. Bueno, J. Catal. 307 (2013) 222–237.
[16] M. Kourtelesis, P. Panagiotopoulou, X.E. Verykios, Catal. Today Part 2 (2015) 247–255.
[17] K.O. Christensen, D. Chen, R. Lødeng, A. Holmen, Appl. Catal. A 314 (2006) 9–22.
[18] F. Haga, T. Nakajima, K. Yamashita, S. Mishima, React. Kinet. Catal. Lett. 63 (1998) 253–259.
[19] I.I. Soykal, H. Sohn, D. Singh, J.T. Miller, U.S. Ozkan, ACS Catal. 4 (2014) 585–592.
[20] P. Biswas, D. Kunzru, Int. J. Hydrogen Energy 32 (2007) 969–980.
[21] T.S. Moraes, R.C.R. Neto, M.C. Ribeiro, L.V. Mattos, M. Kourtelesis, X. Verykios, F.B. Noronha, Top. Catal. 58 (2015) 281–294.
[22] N.J. Divins, A. Casanovas, W. Xu, S.D. Senanayake, D. Wiater, A. Trovarelli, J. Llorca, Catal. Today 253 (2015) 99–105.
[23] F. Aupretre, C. Descorme, D. Duprez, D. Casanave, D. Uzio, J. Catal. 233 (2005) 464–477.
[24] H.-S. Roh, A. Platon, Y. Wang, D.L. King, Catal. Lett. 110 (2006) 1–6.
[25] J. Sun, X.-P. Qiu, F. Wu, W.-T. Zhu, Int. J. Hydrogen Energy 30 (2005) 437–445.
[26] N. Laosiripojana, S. Assabumrungrat, Appl. Catal. B 66 (2006) 29–39.
[27] H. Song, U.S. Ozkan, J. Phys. Chem. A 114 (2010) 3796–3801.
[28] P. Ciambelli, V. Palma, A. Ruggiero, Appl. Catal. B 96 (2010) 18–27.
[29] J. Comas, F. Mariño, M. Laborde, N. Amadeo, Chem. Eng. J. 98 (2004) 61–68.
[30] E. Garcia, M. Laborde, Int. J. Hydrogen Energy 16 (1991) 307–312.
[31] A.N. Fatsikostas, D.I. Kondarides, X.E. Verykios, Catal. Today 75 (2002) 145–155.
[32] J. Rass-Hansen, C.H. Christensen, J. Sehested, S. Helveg, J.R. Rostrup-Nielsen, S. Dahl, Green Chem. 9 (2007) 1016–1021.

[33] G. Zhou, L. Barrio, S. Agnoli, S.D. Senanayake, J. Evans, A. Kubacka, M. Estrella, J.C. Hanson, A. Martínez-Arias, M. Fernández-García, J.A. Rodriguez, Angew. Chem. 122 (2010) 9874–9878.
[34] J.P. Breen, R. Burch, H.M. Coleman, Appl. Catal. B 39 (2002) 65–74.
[35] J. Carrasco, L. Barrio, P. Liu, J.A. Rodriguez, M.V. Ganduglia-Pirovano, J. Phys. Chem. C 117 (2013) 8241–8250.
[36] J. Carrasco, D. López-Durán, Z. Liu, T. Duchoň, J. Evans, S.D. Senanayake, E.J. Crumlin, V. Matolín, J.A. Rodríguez, M.V. Ganduglia-Pirovano, Angew. Chem. Int. Ed. 54 (2015) 3917–3921.
[37] S.D. Senanayake, J. Evans, S. Agnoli, L. Barrio, T.-L. Chen, J. Hrbek, J.A. Rodriguez, Top. Catal. 54 (2011) 34–41.
[38] F. Frusteri, S. Freni, V. Chiodo, L. Spadaro, O. Di Blasi, G. Bonura, S. Cavallaro, Appl. Catal. A 270 (2004) 1–7.
[39] F. Soyal-Baltacıoğlu, A.E. Aksoylu, Z.I. Önsan, Catal. Today 138 (2008) 183–186.
[40] J. Kugai, V. Subramani, C. Song, M.H. Engelhard, Y.-H. Chin, J. Catal. 238 (2006) 430–440.
[41] M. Dan, M. Mihet, Z. Tasnadi-Asztalos, A. Imre-Lucaci, G. Katona, M.D. Lazar, Fuel 147 (2015) 260–268.
[42] H.V. Fajardo, L.F.D. Probst, N.L.V. Carreño, I.T.S. Garcia, A. Valentini, Catal. Lett. 119 (2007) 228–236.
[43] L. Jalowiecki-Duhamel, C. Pirez, M. Capron, F. Dumeignil, E. Payen, Catal. Today 157 (2010) 456–461.
[44] Z. Liu, W. Xu, S. Yao, A.C. Johnson-Peck, F. Zhao, P. Michorczyk, A. Kubacka, E.A. Stach, M. Fernández-García, S.D. Senanayake, J.A. Rodriguez, J. Catal. 321 (2015) 90–99.
[45] M. Patel, T.K. Jindal, K.K. Pant, Ind. Eng. Chem. Res. 52 (2013) 15763–15771.
[46] C. Pirez, M. Capron, H. Jobic, F. Dumeignil, L. Jalowiecki-Duhamel, Angew. Chem. Int. Ed. 50 (2011) 10193–10197.
[47] D. Srinivas, C.V.V. Satyanarayana, H.S. Potdar, P. Ratnasamy, Appl. Catal. A 246 (2003) 323–334.
[48] M.H. Youn, J.G. Seo, K.M. Cho, S. Park, D.R. Park, J.C. Jung, I.K. Song, Int. J. Hydrogen Energy 33 (2008) 5052–5059.
[49] B. Zhang, X. Tang, Y. Li, W. Cai, Y. Xu, W. Shen, Catal. Commun. 7 (2006) 367–372.
[50] F. Frusteri, S. Freni, V. Chiodo, S. Donato, G. Bonura, S. Cavallaro, Int. J. Hydrogen Energy 31 (2006) 2193–2199.
[51] C. Zhang, S. Li, G. Wu, J. Gong, Catal. Today 233 (2014) 53–60.
[52] M. Sánchez-Sánchez, R. Navarro, J. Fierro, Int. J. Hydrogen Energy 32 (2007) 1462–1471.
[53] A. Lucrédio, J. Bellido, E. Assaf, Appl. Catal. A 388 (2010) 77–85.
[54] J. Ye, Y. Wang, Y. Liu, H. Wang, Int. J. Hydrogen Energy 33 (2008) 6602–6611.
[55] S. QiuJie, L. Chengwei, C. Weiqing, J. Rare Earths 27 (2009) 948–954.
[56] F. Liu, L. Zhao, H. Wang, X. Bai, Y. Liu, Int. J. Hydrogen Energy 39 (2014) 10454–10466.
[57] Z. Liu, T. Duchoň, H. Wang, E.W. Peterson, Y. Zhou, S. Luo, J. Zhou, V. Matolín, D.J. Stacchiola, J.A. Rodriguez, S.D. Senanayake, J. Phys. Chem. C 119 (2015) 18248–18256.
[58] W. Xu, Z. Liu, A.C. Johnston-Peck, S.D. Senanayake, G. Zhou, D. Stacchiola, E.A. Stach, J.A. Rodriguez, ACS Catal. 3 (2013) 975–984.
[59] L. Jalowiecki-Duhamel, C. Pirez, M. Capron, F. Dumeignil, E. Payen, Int. J. Hydrogen Energy 35 (2010) 12741–12750.
[60] Y. Zhou, J. Zhou, J. Phys. Chem. C 116 (2012) 9544–9549.
[61] Y. Zhou, J.M. Perket, A.B. Crooks, J. Zhou, J. Phys. Chem. Lett. 1 (2010) 1447–1453.
[62] H. Song, U.S. Ozkan, J. Catal. 261 (2009) 66–74.
[63] S.M. de Lima, I.O. da Cruz, G. Jacobs, B.H. Davis, L.V. Mattos, F.B. Noronha, J. Catal. 257 (2008) 356–368.
[64] S. Sinharoy, L.L. Levenson, Thin Solid Films 53 (1978) 31–36.
[65] G. Meyer, F.E.C. Scheffer, J. Am. Chem. Soc. 75 (1953) 486.
[66] M. Sarr, N. Bahlawane, D. Arl, M. Dossot, E. McRae, D. Lenoble, J. Phys. Chem. C 118 (2014) 23385–23392.
[67] L.J.E. Hofer, E.M. Cohn, W.C. Peebles, J. Phys. Colloid Chem. 54 (1950) 1161–1169.
[68] X.Z. Du, L. Dong, C. Li, Y.Q. Liang, Y. Chen, Langmuir 15 (1999) 1693–1697.
[69] A. Yee, S.J. Morrison, H. Idriss, J. Catal. 191 (2000) 30–45.
[70] C. Li, Y. Sakata, T. Arai, K. Domen, K. Maruya, T. Onishi, J. Chem. Soc. Farad. Trans. 1. 85 (1989) 929–943.
[71] C. Li, Y. Sakata, T. Arai, K. Domen, K.I. Maruya, T. Onishi, J. Chem. Soc. Farad. Trans. 1. 85 (1989) 1451–1461.
[72] H. Song, L.Z. Zhang, R.B. Watson, D. Braden, U.S. Ozkan, Catal. Today 129 (2007) 346–354.
[73] D.R. Mullins, P.M. Albrecht, T.-L. Chen, F.C. Calaza, M.D. Biegalski, H.M. Christen, S.H. Overbury, J. Phys. Chem. C 116 (2012) 19419–19428.
[74] A. Yee, S.J. Morrison, H. Idriss, J. Catal. 186 (1999) 279–295.
[75] B. Bayram, I.I. Soykal, D. von Deak, J.T. Miller, U.S. Ozkan, J. Catal. 284 (2011) 77–89.
[76] K.V. Manukyan, A.J. Cross, A.V. Yeghishyan, S. Rouvimov, J.J. Miller, A.S. Mukasyan, E.E. Wolf, Appl. Catal. A 508 (2015) 37–44.
[77] A.L. Alberton, M.M.V.M. Souza, M. Schmal, Catal. Today 123 (2007) 257–264.
[78] A. Carrero, J.A. Calles, A.J. Vizcaíno, Appl. Catal. A 327 (2007) 82–94.
[79] S. Helveg, C. Lopez-Cartes, J. Sehested, P.L. Hansen, B.S. Clausen, J.R. Rostrup-Nielsen, F. Abild-Pedersen, J.K. Norskov, Nature 427 (2004) 426–429.
[80] K. Hata, D.N. Futaba, K. Mizuno, T. Namai, M. Yumura, S. Iijima, Science 306 (2004) 1362–1364.
[81] S. Gates, J. Russell, J. Yates, Surf. Sci. 171 (1986) 111–134.
[82] J. Xu, X. Zhang, R. Zenobi, J. Yoshinobu, Z. Xu, J.T. Yates, Surf. Sci. 256 (1991) 288–300.
[83] T. Kratochwil, M. Wittmann, J. Küppers, J. Electron. Spectrosc. Relat. Phenom. 64 (1993) 609–617.
[84] M.C. Wu, C.M. Truong, D.W. Goodman, J. Phys. Chem. 97 (1993) 9425–9433.
[85] D.R. Mullins, S.D. Senanayake, T.L. Chen, J. Phys. Chem. C 114 (2010) 17112–17119.
[86] D.E. Gordon, R.M. Lambert, Surf. Sci. 287 (1993) 114–118.
[87] L. Cederbaum, W. Domcke, W. Von Niessen, W. Brenig, Z. Phys. B Con. Matter 21 (1975) 381–388.
[88] G.J. Kovács, I. Bertóti, G. Radnóczi, Thin Solid Films 516 (2008) 7942–7946.
[89] I. Czekaj, F. Loviat, F. Raimondi, J. Wambach, S. Biollaz, A. Wokaun, Appl. Catal. A 329 (2007) 68–78.
[90] C. Ducati, I. Alexandrou, M. Chhowalla, J. Robertson, G.A.J. Amaratunga, J. Appl. Phys. 95 (2004) 6387–6391.
[91] C. Klink, I. Stensgaard, F. Besenbacher, E. Lægsgaard, Surf. Sci. 342 (1995) 250–260.
[92] R.S. Weatherup, L. D'Arsié, A. Cabrero-Vilatela, S. Caneva, R. Blume, J. Robertson, R. Schloegl, S. Hofmann, J. Am. Chem. Soc. 137 (2015) 14358–14366.
[93] T. Tanaka, K.N. Ishihara, P.H. Shingu, Metall. Trans. A 23 (1992) 2431–2435.
[94] O. Skoplyak, M.A. Barteau, J.G. Chen, J. Phys. Chem. B 110 (2006) 1686–1694.
[95] F.P. Netzer, T.E. Madey, J. Chem. Phys. 76 (1982) 710–715.
[96] H. Öfner, F. Zaera, J. Phys. Chem. B 101 (1997) 9069–9076.
[97] L. Surnev, Z. Xu, J.T. Yates Jr., Surf. Sci. 201 (1988) 1–13.
[98] L. Barrio, A. Kubacka, G. Zhou, M. Estrella, A. Martínez-Arias, J.C. Hanson, M. Fernández-García, J.A. Rodriguez, J. Phy. Chem. C 114 (2010) 12689–12697.
[99] C. Pirez, W. Fang, M. Capron, S. Paul, H. Jobic, F. Dumeignil, L. Jalowiecki-Duhamel, Appl. Catal. A (2015), http://dx.doi.org/10.1016/j.apcata.2015.10.035.
[100] W. Fang, C. Pirez, S. Paul, M. Capron, H. Jobic, F. Dumeignil, L. Jalowiecki-Duhamel, ChemCatChem 5 (2013) 2207–2216.
[101] J.A. Rodriguez, J.C. Hanson, J.-Y. Kim, G. Liu, A. Iglesias-Juez, M. Fernández-García, J. Phys. Chem. B 107 (2003) 3535–3543.
[102] M. Ozawa, M. Kimura, A. Isogai, J. Alloys Compd. 193 (1993) 73–75.
[103] Y. Nagai, T. Yamamoto, T. Tanaka, S. Yoshida, T. Nonaka, T. Okamoto, A. Suda, M. Sugiura, Catal. Today 74 (2002) 225–234.
[104] M. Tada, S. Zhang, S. Malwadkar, N. Ishiguro, J.-i. Soga, Y. Nagai, K. Tezuka, H. Imoto, S. Otsuka-Yao-Matsuo, S.-i. Ohkoshi, Y. Iwasawa (Eds.), Angew. Chem. Int. Ed. 51 (2012) 9361–9365.
[105] T. Yamamoto, A. Suzuki, Y. Nagai, T. Tanabe, F. Dong, Y. Inada, M. Nomura, M. Tada, Y. Iwasawa, Angew. Chem. Int. Ed. 46 (2007) 9253–9256.
[106] S. Bernal, G. Blanco, M.A. Cauqui, P. Corchado, J.M. Pintado, J.M. Rodríguez-Izquierdo, Chem. Commun. (1997) 1545–1546.
[107] B.M. Reddy, L. Katta, G. Thrimurthulu, Catal. Today 175 (2011) 585–592.
[108] A. Martínez-Arias, A. Hungría, M. Fernández-García, A. Iglesias-Juez, J. Soria, J. Conesa, J. Anderson, G. Munuera, Phys. Chem. Chem. Phys. 14 (2012) 2144–2151.
[109] A. Hornés, P. Bera, A.L. Cámara, D. Gamarra, G. Munuera, A. Martínez-Arias, J. Catal. 268 (2009) 367–375.
[110] A. Hornés, D. Gamarra, G. Munuera, J. Conesa, A. Martínez-Arias, J. Power Sour. 169 (2007) 9–16.
[111] J.A. Rodriguez, X. Wang, J.C. Hanson, G. Liu, A. Iglesias-Juez, M. Fernández-Garcıía, J. Chem. Phys. 119 (2003) 5659–5669.
[112] W. Huang, P. Shuk, M. Greenblatt, Chem. Mater. 9 (1997) 2240–2245.
[113] S. Bernal, G. Blanco, M.A. Cauqui, G.A. Cifredo, J.M. Pintado, J.M. Rodriguez-Izquierdo, Catal. Lett. 53 (1998) 51–57.
[114] L. Pino, A. Vita, F. Cipitì, M. Laganà, V. Recupero, Appl. Catal. B 104 (2011) 64–73.
[115] A. Bueno-López, K. Krishna, M. Makkee, J. Moulijn, J. Catal. 230 (2005) 237–248.
[116] F. Moreau, G.C. Bond, B. van der Linden, B.A. Silberova, M. Makkee, Appl. Catal. A 347 (2008) 208–215.
[117] H.S. Bengaard, J.K. Nørskov, J. Sehested, B. Clausen, L. Nielsen, A. Molenbroek, J. Rostrup-Nielsen, J. Catal. 209 (2002) 365–384.
[118] J.R. Rostrup-Nielsen, J. Sehested, J.K. Nørskov, Hydrogen and synthesis gas by steam- and C02 reforming, Adv Catal, Academic Press, (2002), pp. 65–139.